PHYSICS OF FLUIDS **28**, 096602 (2016)

Gravity currents in a linearly stratified ambient fluid created by lock release and influx in semi-circular and rectangular channels

S. Longo,[1,a)] M. Ungarish,[2] V. Di Federico,[3] L. Chiapponi,[1] and F. Addona[1]
[1]*Dipartimento di Ingegneria Civile, Ambiente Territorio e Architettura (DICATeA), Università di Parma, Parco Area delle Scienze, 181/A, 43124 Parma, Italy*
[2]*Department of Computer Science, Technion – Israel Institute of Technology, Haifa 32000, Israel*
[3]*Dipartimento di Ingegneria Civile, Chimica, Ambientale e dei Materiali (DICAM), Università di Bologna, Viale Risorgimento, 2, 40136 Bologna, Italy*

(Received 24 July 2016; accepted 5 September 2016; published online 29 September 2016)

We present an experimental investigation, supported by a theoretical model, of the motion of lock-release, constant inflow, and time varying inflow gravity currents (GCs) into a linearly stratified ambient fluid at large Reynolds number. The aim is the experimental validation of a simple model able to predict the slumping phase front speed and the asymptotic self-similar front speed for rectangular and circular cross section channels. The first investigated system is of Boussinesq type with the dense current (salt water dyed with aniline) released in a circular channel of 19 cm diameter and 400 cm long (605 cm in the inflow experiments), half-filled of linearly stratified ambient fluid (salt water with varying salt concentration). The second system has the same components but with a channel of rectangular cross section of 14 cm width, 11 cm ambient fluid depth, and 504 cm length. The density stratification of the ambient fluid was obtained with a computer controlled set of pumps and of mixing tanks. For the experiments with inflow, a multi-pipes drainage system was set at the opposite end with respect to the inflow section, computer controlled to avoid the selective withdrawal. The numerous experiments (28 for circular cross section, lock release; 26 for circular and 14 for rectangular cross section, constant inflow (fluid volume $\propto t^{\alpha}$, with $\alpha = 1$); 6 for circular cross section, linearly increasing inflow ($\alpha = 2$)), with several combination of the stratification parameter ($0 < S < 1$) confirm the theory within ≈30% (≈40% for a single series of experiments), which is considered a good result in view of the various underlying simplifications and approximations. The results on the front speed of the GCs are discussed in the presence of the internal waves, which have a celerity given by a theoretical and experimentally tested model for the rectangular but not for the circular cross section. The theoretical analysis of internal waves in circular cross sections has been extended and experimentally validated. *Published by AIP Publishing.* [http://dx.doi.org/10.1063/1.4963009]

I. INTRODUCTION

Gravity currents (GCs) consist of a primarily horizontal flow driven by a density difference, hence the alternative name of "density currents." Typically, their aspect ratio is very small, as the horizontal length scale is much larger than the vertical; correspondingly, vertical accelerations of fluid particles tend to be negligible with respect to horizontal, leading to the hydrostatic approximation for the pressure.

Gravity currents can be classified according to dominant forces (inviscid or viscous), the type of release (instantaneous or continuous), and the degree of density difference between the fluids

a)Author to whom correspondence should be addressed. Electronic mail: sandro.longo@unipr.it

(Boussinesq or non-Boussinesq). The study of high-Reynolds-number (almost) inviscid gravity currents, dominated by the interplay of inertial and buoyancy forces, has been motivated by the need to understand a variety of environmental phenomena. Typical examples are turbidity currents in natural water bodies, sea breezes, avalanches, and lava and pyroclastic flows. As such, a vast literature exists on the topic (Simpson,[22] Ungarish[25]). The pioneering works of Benjamin,[3] Huppert and Simpson,[9] and Rottman and Simpson[20] dealt with the reference case of a steady or unsteady gravity current advancing in a wide rectangular channel; later, many different authors introduced complexity and refinements at various levels, in an attempt to capture more realistically the behaviour of natural currents. These often interact with channel topography (as for tidal intrusions, mudflows, and gas flow in tunnels) or advance into an ambient fluid with spatially variable density, typically in the form of a vertical density stratification (as in the atmosphere, lakes, and oceans). At large scales, the rotation of the reference system has important effects on the dynamics of the gravity currents, see, e.g., the work of Mahalov *et al.*[16] and Hunt *et al.*[8]

As for topographic control, the constraint introduced by boundaries significantly modifies the rate of advance of the gravity current. The front condition for steady currents in non-rectangular channels of assigned cross section was investigated theoretically and experimentally by Marino and Thomas,[17] and theoretically by Ungarish.[27,30] The propagation of lock-exchange unsteady currents in V-shaped channels was investigated experimentally and with a box model by Monaghan *et al.*[19] Zemach and Ungarish[35] developed a one-layer model for unsteady lock-release flow for a generic non-rectangular cross section; a two-layer model for the same problem was presented by Ungarish.[28] An experimental confirmation, including theoretical refinements, of the latter model was obtained by Ungarish *et al.*[32] for a V-shaped channel, and by Longo *et al.*[14] for a circular channel. A further extension of the model to currents with constant and variable inflow is reported in the work of Longo *et al.*,[13] together with experimental confirmation in both conditions.

The importance of fluid stratification can be understood by recalling that according to Yih,[34] the most interesting features of the dynamics of non-homogeneous fluids reside in their association with gravity effects; the interplay of heterogeneity and gravity produces striking phenomena entirely unexpected. The effect of fluid stratification, mostly taken to be linear, has been studied almost exclusively in association with planar gravity currents. A generalization of the front condition to stratified ambient was developed by Ungarish[24] and Flynn *et al.*[6] for steady currents, respectively in the context of one- and two-layer models. Spreading of lock-exchange currents was investigated experimentally by Maxworthy *et al.*;[18] these experiments validated the one-layer theoretical model developed independently by Ungarish and Huppert.[31] The latter theory was further extended by Ungarish[26] to systems in which both the intruding current and ambient fluid are stratified.

There are some important motivations to extend the analysis of gravity currents to a non-rectangular cross section. It has been verified (see, e.g., White and Helfrich[33]) that 2-D simulations of rectangular cross section gravity currents give results which favourably compare with the experiments, hence we infer that for this geometry, all the three dimensional phenomena (e.g., vorticity dynamics) have a minor relevance. A non-rectangular cross section implies a truly three dimensional behaviour of the advancing current and of the ambient fluid. An experimental confirmation in 3-D of the simplified theoretical model is requested to acquire confidence in the goodness of the approximations and of the simplifications also in flow fields wherein turbulence energy exchanges and vorticity dynamics play an important role. In addition, a rectangular cross section (which also mimics an infinite plane) is seldom representative of natural situations: for instance, V-shaped and U-shaped (locally approximated by a parabola or a circular half-filled cross section) cross sections are typical of submarine canyons (see, e.g., the work of Inman *et al.*[10] and Covault *et al.*[4]).

Not infrequently, topographic control and ambient fluid stratification are simultaneously present, as in the dynamics of the atmosphere, oceans, and lakes. To understand the mutual influence of the two factors, Ungarish[29] developed a one-layer model for lock-exchange currents subject to the influence of both stratification (expressed by the dimensionless parameter $S \in [0,1]$) and geometry of the cross section. This approach, valid for a linearly stratified ambient fluid and a general shape of the cross section of the channel, constitutes a generalization of earlier formulations. While the resulting shallow water (SW) equations are amenable in general to a numerical solution by finite

difference methods, the initial slumping phase can be solved with the method of characteristics, and at large times, a self-similar regime may develop.

A general observation is that a quite comprehensive SW theory is now available for the prediction of gravity currents in a wide range of circumstances: channels of various cross section, with homogeneous or stratified ambients, with and without influx (constant or time dependent). This is a very significant extension of the classical theory which covered gravity currents in rectangular (or laterally unbounded) channels. In the novel theory, the classical configuration is just a particular case with a constant width function of the height ($f(z)$ = const.). Needless to say, such a widening of the range of applicability of the theoretical framework requires careful experimental verifications and assessment. The present study is expected to contribute to this corroboration effort.

To the best of our knowledge, the aforementioned theoretical shallow-water model was never directly tested experimentally to investigate its validity nor was it extended to currents produced by the release of a constant inflow (as opposed to lock-release currents), despite these currents being common in environmental applications. This paper aims at bridging these gaps in the existing experimental and theoretical knowledge of inviscid gravity currents. To this end, we first present in Sec. II an extension of the formulation by Ungarish[29] to the constant inflow case and to the long-term self-similar regime. We then report in Sec. III results stemming from an extensive experimental investigation involving the following: (1) lock-release experiments in a circular channel, aimed at testing the validity of Ungarish's[29] formulation; (2) constant inflow experiments in rectangular and circular channels, geared at supporting the new theoretical developments of Sec. II; (3) time varying inflow experiments with $S = 0, 1$ in circular channels, to verify the theoretical self-similar solutions. Appendix A presents some details on the geometry of circular cross sections; Appendix B illustrates the computation of the first mode internal wave celerity for a circular channel; Appendix C shows the experimental setup to measure the internal waves celerity in a circular channel, and some measurements of the internal wave density patterns for two experiments in the supercritical and subcritical regimes, respectively.

II. THEORETICAL MODEL

The geometry of the cross section is represented by the width-function $f(z)$, $0 \le z \le H$. The standard rectangular cross section channel corresponds to $f(z)$ = const. (see the schematic description in Figure 1). The circular form of our system renders $f(z) = 2(2r)^{1/2}z^{1/2}[1 - z/(2r)]^{1/2}$, $0 \le z \le H \le 2r$. (Note that $f(z) = 2(2r)^{1/2}z^{1/2}$ is a good approximation for small z/r.)

Let A, A_a, and A_T denote the cross section area of the current, ambient, and the total of the channel. The relevant definitions (see Figure 1) are

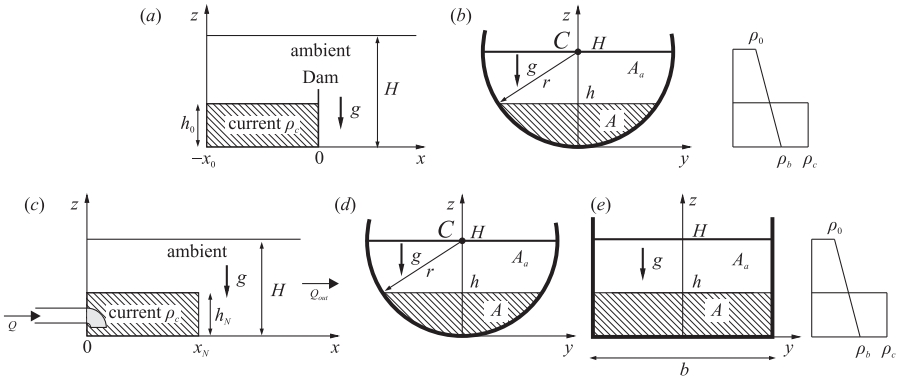

FIG. 1. A schematic description of the (a) lock-release problem for the (b) circular cross section and of the inflow problem (c) for the (d) circular cross section (for $\beta = H/r = 1$) and for the (e) rectangular cross section. C is the center and r is the radius, b is the width of the rectangular channel, g is the acceleration of gravity, H is the ambient fluid depth, h is the dense current height, h_0 is the initial depth of the dense current in the lock, Q is the inflow rate, ρ_0 and ρ_b are the ambient fluid mass density at $z = H$ and at $z = 0$, respectively, with a linear variation along the vertical, and ρ_c is the mass density of the current.

$$A = A(h) = \int_0^h f(z)dz, \quad A_T = \int_0^H f(z)dz, \quad A_a = A_T - A. \tag{1}$$

Note that

$$\frac{\partial A}{\partial x} = f(h)\frac{\partial h}{\partial x}; \quad \frac{\partial A}{\partial t} = f(h)\frac{\partial h}{\partial t}. \tag{2}$$

An important variable in the formulation is the area ratio of current to total (channel),

$$\varphi = \varphi(h) = A/A_T, \tag{3}$$

which for the 2-D case is simply $a = h/H$. The calculation of $\varphi(h)$ (and of other related geometrical expressions) for the circular channel is briefly discussed in Appendix A.

We introduce the averaged velocity $u(x,t)$ for the current and $u_a(x,t)$ for the ambient. The averaging is over the corresponding areas. The continuity equation for the current expresses the observation that the upward flux $f(h)(\partial h/\partial t)$ is balanced by $-\partial(Au)/\partial x$. This can be rewritten as

$$\frac{\partial A}{\partial t} + \frac{\partial uA}{\partial x} = 0; \quad \text{or} \quad \frac{\partial h}{\partial t} + u\frac{\partial h}{\partial x} + \frac{A}{f(h)}\frac{\partial u}{\partial x} = 0. \tag{4}$$

For the ambient layer, continuity yields

$$u_a A_a = -uA. \tag{5}$$

The flow in the ambient is also called "return flow," and is considered a by-product of the main flow of the current. The effect of the return flow is small when $\rho_a u_a \ll \rho_c u$.

In many cases of interest, the GC is thin with respect to the ambient, and the density differences between the current and ambient are relatively small. This allows for a useful simplification of the high-Reynolds number equations of motion, referred to as one-layer SW Boussinesq model.

From the physical point of view, (i) the effect of the "return" flow in the ambient above the current is neglected, i.e., $u_a = 0$, as if $h/H \to 0$. However, for the calculation of Fr at the nose, a finite h_N/H is taken, according to the system under consideration; (ii) the difference between ρ_c and ρ_a is assumed negligibly small in the inertia terms, but relevant in the reduced gravity g' which is the driving effect.

We consider the case of a linearly stratified ambient, whose density increases from ρ_b at the bottom $z = 0$ to ρ_0 at the top $z = H$. This is expressed as

$$\rho_c = \rho_0(1+\epsilon), \quad \rho_a(z) = \rho_0\left[1 + \epsilon\, S\left(1 - \frac{z}{H}\right)\right], \tag{6}$$

where

$$\epsilon = \frac{\rho_c - \rho_0}{\rho_0}, \quad S = \frac{\rho_b - \rho_0}{\rho_c - \rho_0}, \quad g' = \epsilon\, g. \tag{7}$$

The parameter $S \in [0,1]$ represents the stratification of the ambient. Conveniently, the non-stratified case is obtained by setting $S = 0$ in the equations. $S = 1$ is the maximum stratification, $\rho_c = \rho_b$ case. For stratified fluid, the buoyancy frequency $N^2 = -(g/\rho)\partial\rho/\partial z = Sg'/H$ is defined.

Consider the pressure fields p_i, $i = a, c$ (in the ambient and current, respectively). The thin-layer assumption predicts that for both fluids, the dominant z-momentum balance is the hydrostatic, $\partial p_i/\partial z = -\rho_i g$, and the pressure is continuous at the interface $z = h$. Using the appropriate densities, we obtain

$$p_a(z) = -\rho_0 g\left[1 + \epsilon\, S\left(1 - \frac{z}{2H}\right)\right] z + \mathrm{C}, \tag{8}$$

$$p_c = -\rho_0 g(1+\epsilon)(z-h) + p_a(h), \tag{9}$$

where C is a constant and $h = h(x,t)$. The driving effect is the $x-$component of the pressure gradient, which follows from Eq. (9) as

$$\frac{\partial p_c}{\partial x} = g'\rho_0\left(1 - S + S\frac{h}{H}\right)\frac{\partial h}{\partial x}. \tag{10}$$

We average the x-momentum inviscid equation over the area A. The balance is between inertia and pressure gradient (buoyancy). The inertial term $\rho_c Du/Dt$ is like in the non-stratified case, and the averaged pressure-gradient term is given by Eq. (10) (which is constant over A). With the $\rho_c \approx \rho_0$ (i.e., $\epsilon \ll 1$) Boussinesq approximation, we thus obtain the momentum equation as

$$\frac{\partial u}{\partial t} + u\frac{\partial u}{\partial x} = -g'\left(1 - S + S\frac{h}{H}\right)\frac{\partial h}{\partial x}. \tag{11}$$

Hereafter, we use *dimensionless* variables unless stated otherwise. We scale horizontal lengths along the channel with x_0, vertical lengths with h_0, width with $f(h_0)$, speed with U, and time with T, where

$$U = (g'h_0)^{1/2}, \quad T = x_0/U. \tag{12}$$

The nose $x = x_N$ is a discontinuity governed by the jump condition

$$u_N = Fr\, h_N^{1/2}\Psi^{1/2}, \tag{13}$$

where (i) the "Froude number" function is provided by the generalization of Benjamin's result (see the work of Ungarish[27]),

$$Fr^2 = \frac{2(1-\varphi)}{1+\varphi}\left(1 - \varphi + \frac{1}{hA_T}\int_0^h z f(z)dz\right), \tag{14}$$

and (ii) the stratification coefficient is estimated as the ratio of pressure-force over the nose with and without stratification,

$$\Psi = \frac{\int_0^{h_N}[(p_c - p_a)_S]\ f(z)dz}{\int_0^{h_N}[(p_c - p_a)_{S=0}]\ f(z)dz}. \tag{15}$$

Using Eqs. (8) and (9), we obtain

$$\Psi = 1 - S\left[1 - \frac{1}{2}\frac{h_N}{H}(1+\Gamma)\right], \tag{16}$$

$$\Gamma = \frac{\int_0^{h_N}(z/h_N)(h_N - z)\, f(z)dz}{\int_0^{h_N}(h_N - z)\, f(z)dz}. \tag{17}$$

Note that $0 < \Gamma < 1$, dependent on the cross section shape (for 2-D case $\Gamma = 1/3$, for the circle $\Gamma \approx 0.43$). As could be anticipated, the stratification slows down the propagation: $\Psi = 1$ for $S = 0$, and decreases with S.

The dimensionless equation of continuity is Eq. (4) (unchanged), and of momentum is Eq. (11) with g' removed. The system for $h(x,t), u(x,t)$ is hyperbolic, and the characteristic balances are

$$G(h)dh \pm du = 0 \quad \text{on} \quad \frac{dx}{dt} = c_\pm = u \pm \left[\Theta(h)\left(1 - S + S\frac{h}{H}\right)\right]^{1/2}, \tag{18}$$

where

$$\Theta(h) = \frac{A}{f(h)}, \quad G(h) = \left[\frac{1}{\Theta(h)}\left(1 - S + S\frac{h}{H}\right)\right]^{1/2}. \tag{19}$$

In general, the equations of motion must be solved numerically. However, some analytical solutions are available, as discussed below.

A. Lock-release (fixed volume) slumping

For the lock-release problem, the initial conditions at $t = 0$ are $u = 0, h = 1$ in the lock $0 \le x < 1$, $x_N = 1$. The boundary condition at the reservoir backwall $x = 0$ is $u = 0$.

The motion starts with the slumping phase with constant speed u_N and height h_N. To determine these values, we integrate du/dh from Eq. (18) on a c_+ characteristic, from the reservoir with $(0,1)$ initial conditions to the nose with (u_N, h_N) conditions. We intersect the $u(h)$ produced by the integration with the front condition (13) to obtain

$$u_N \equiv \int_{h_N}^{1} G(h)dh = Fr\,(h_N)h_N^{1/2}\left(1 - S\left[1 - \frac{1}{2}\frac{h_N}{H}(1+\Gamma)\right]\right)^{1/2}, \tag{20}$$

where $G(h)$ is given by Eq. (19). With the outcome represented by Eq. (20), we first solve for h_N, then obtain u_N. The shape of the cross section enters into the expressions G, Fr, and Γ. The solution is obtained by standard numerical methods (e.g., Romberg integration and a secant-method solver). Such results are considered "exact" and serve as reliable tests for solutions of the SW equations obtained by finite-difference codes. The slumping results are relevant for a propagation to about $x_N = 3$, during which a c_- characteristic from the gate $(t = 0, x = 1)$ travels to backwall, is reflected, and then reaches the nose with the information that the boundary conditions require a decrease of u_N.

B. Fixed inflow rate

When the current is sustained by a fixed (constant) inflow (source) at rate Q at $x = 0$, a possible solution is a current with constant h_N and u_N. Now the outflux (sink) conditions from the tank are significant. We introduce the parameter $\gamma \in [0,1]$. Assume that γQ is withdrawn at $x = 0$ and $(1-\gamma)Q$ at the opposite end. The $\gamma = 0$ situation is called "no return," because there is no flow of ambient above the current. In the inflow case x_0, h_0 of the lock are missing; for definiteness we set $x_0 = h_0 = H$. In other words, the scaling length in both horizontal and vertical directions is the height of the ambient fluid, and influx rate Q is scaled with H^2U.

The current flows like a slug of height and speed h_N, u_N and hence volume continuity is expressed as

$$A(h_N)u_N = Q. \tag{21}$$

The nose jump condition (13) was written for a current that propagates into an unperturbed (stationary) ambient. In the present system the ambient moves with velocity $(1-\gamma)Q/A_T$, and hence, following Shringarpure *et al.*[21] and Longo *et al.*,[14] the jump condition must be applied to the relative motion, i.e.,

$$u_N - (1-\gamma)Q/A_T = Fr\,h_N^{1/2}\Psi^{1/2}. \tag{22}$$

Combining Eqs. (21) and (22), with the auxiliary Eqs. (14)-(16), we obtain h_N and u_N. The dimensionless input parameters for the solution are the stratification parameter S, the inflow rate Q, and the fraction of return flow, γ. For the circle, we also must provide $\beta = H/r$ (ratio of height of ambient to radius). In a real system the Reynolds number is also available, $Re = UH/\nu_c$, where ν_c is the kinematic viscosity of the current.

C. Similarity solutions

We consider gravity currents of volume $\mathcal{V} = Qt^\alpha$. The fixed flux case, $\alpha = 1$, is excepted from this discussion. The reason is that the results derived above for this case are already a similarity solution. The similarity solutions for $\alpha \neq 1$ must be subjected to various restrictions, and are considered separately.

After significant propagation, the influence of the initial conditions diminishes, and the ratio h_N/H is sufficiently small to justify a constant $Fr = Fr(0)$ approximation. We seek a similarity solution of the form

$$x_N = Kt^\delta, \quad h(\xi,t) = \Omega(t)\mathcal{H}(\xi), \quad u(\xi,t) = \dot{x}_N\mathcal{U}(\xi), \tag{23}$$

where $\xi = x/x_N(t)$, the upper dot means time derivative, and K, δ are positive constants. The boundary conditions are $\mathcal{U}(1) = 1$, Eq. (13), and volume conservation,

$$\mathcal{V} = \int_0^{x_N} A(h)dx = x_N\int_0^1 A[\Omega(t)\mathcal{H}(\xi)]d\xi = Qt^\alpha. \tag{24}$$

The fixed-volume case corresponds to $\alpha = 0, Q = \mathcal{V}_0$.

The analysis proves that such similarity solution exists only under the following restrictions (the exception is the constant-flux $\alpha = 1$ current). First, we must use a power-law cross section, $f(z) = z^\sigma$ (the standard $f(z) = 1$ included), with $\mathcal{V}_0 = 1/(\sigma + 1)$. In this case, $A(h) = h^{1+\sigma}/(1 + \sigma)$, and the integral in Eq. (24) attains a self-similar form. Second, the ambient is either homogeneous $S = 0$ or with maximum stratification $S = 1$. This is needed to obtain the similarity form of the u_N condition. Under these conditions, solutions can be obtained with

$$\delta = (2\sigma + 2 + \alpha)/(2\sigma + 3) \quad \text{for} \quad S = 0, \tag{25}$$

$$\delta = (\sigma + 1 + \alpha)/(\sigma + 2) \quad \text{for} \quad S = 1. \tag{26}$$

In particular, simple analytical self-similar solutions are obtained for $\alpha = 0$. For more details see the work of Zemach and Ungarish,[35] Sec. V, and Ungarish,[29] Sec. 5 (note the rescaling (5.1) there).

The similarity solutions are relevant to the experiments under consideration in this paper: power-law $f(z) = bz^\sigma$ with $\sigma = 1/2$ approximates the circular channel under consideration in this paper, while $\sigma = 0$ reproduces the rectangular cross section. The theoretical exponents are $\delta = 3/4$ and $\delta = 3/5$ for the lock-release experiments in the circular cross section channel for $S = 0$ and $S = 1$, respectively. For $\alpha = 2$ the theoretical exponent for $S = 0, 1$ is $\delta = 5/4, 7/5$, respectively.

Again, a notable exception is the constant-flux $\alpha = 1$ current. In this case $\Omega = \text{const.}, \delta = 1$, and some of the previous restrictions can be relaxed. The slug-like self-similar propagation with constant h_N, u_N, see Sec. II B, is an exact solution for a general $f(z)$, any S, and finite h_N/H.

The main deficiency of the similarity solutions is the vague connection with realistic initial/boundary conditions of the current. For example, (i) in the lock-released current the shift of t by a constant to a "virtual origin" does not affect the solution; (ii) for constant inflow, the theoretical height and speed at the source must be the same as at the nose, and this is incompatible with inflow conditions in practical systems. The assumption is that the similarity solutions are applicable after some adjustment in time or distance.

D. Internal waves

A peculiar characteristic of GCs propagating in a density stratified fluid is the generation of internal waves which can interact with the current modifying its behaviour in a complex manner. The advancing nose of the current displaces the isopycnal layers, and the disturbance propagates with a celerity related to the density stratification and to the geometry of the ambient fluid. The fastest internal waves in straight channels of depth varying only in the transverse direction are the long waves with $k \to 0$, where k is the wavenumber, because $dc^2/dk^2 < 0$ (see Ref. 34, Theorem 2 in Sec. 17). Since in many practical situations the GCs front speed is comparable with the internal wave celerity, two regimes of propagation are forecast: (i) supercritical if $u_N > c$, and (ii) subcritical if $u_N < c$. Extensive analysis on the effects of stratification of GC speed was performed by Ungarish[24] with subsequent extension by Helfrich.[33] The comparison with the experiments by Maxworthy *et al.*[18] of lock-released GCs in a linearly stratified ambient fluid indicates that supercritical currents are essentially not influenced by the internal waves, which propagate behind the front and eventually modify the shape of the current, enhancing mixing. For subcritical GCs the scenario looks different, with the current experiencing an inviscid interaction with the internal waves; the interaction is presently not described by the SW solution. The current experiences a strong deceleration when coupling with internal waves is at a maximum, and eventually recovers its previous speed.

However, it appears that except for the speed and the height, the GCs are slightly influenced by the internal wave generation, with a limited transfer of energy from the current toward the internal waves (Ungarish and Huppert[31]). In order to explain experimental results, a comparison of the front speed and of the wave celerity is suggested. While for a rectangular cross section channel with linear stratification the fundamental mode celerity is given in Ref. 2 as $c_{rect} = NH/\pi$ (dimensional values), for a circular cross section channel the analysis by Yih[34] is rich in details for the different modes but is lacking the dispersion relation. Hence, the analysis by Yih[34] has been extended in the present paper (see Appendix B), and the fundamental mode celerity is found equal to $c = Nr/(2\sqrt{2})$

(dimensional values). A series of experiments (see Appendix C) have been performed to measure the internal waves celerity in the circular cross section channel in order to verify the theory.

In summary, while analyzing the experimental results we must keep in mind the fundamental simplifications underlying the mathematical model: the current is a thin layer; the pressure is hydrostatic; there is pressure continuity at the interface, except for the jump at the front (nose); viscous effects inside the current and at the boundaries are negligible (large Reynolds number); the system is Boussinesq; the stratification of the ambient is linear; no mixing and entrainment effects are considered; and no coupling between GC and internal waves is modeled, in both subcritical and supercritical regimes. Moreover, here we use a "one-layer model" which neglects the dynamic effects of the "return" flow in the ambient above the current.

III. THE EXPERIMENTS

A. Experimental setup and methodology

A series of experiments were performed to test the validity of the SW mathematical models for the gravity current propagating into a stratified ambient fluid, both in rectangular and non-rectangular geometries. To this end, lock-release and constant inflow experiments were carried out in a circular transparent thermoplastic tube of internal radius $r = 9.5$ cm and total length 605 cm for constant inflow experiments and 500 cm for lock-release experiments; in the latter case, the lock length was 100 cm (see Ref. 14 for additional details). A second set of constant inflow experiments was carried out in a rectangular PVC channel of $14 \times 14\,\text{cm}^2$ cross section and length 504 cm. See Figure 2 for the different setups. A third set of experiments was carried out in the circular cross section channel ($r = 9.5$ cm and total length 605 cm) for linearly increasing inflow ($\alpha = 2$) to test self-similar solutions for $S = 0, 1$.

The density stratification of the fluid was obtained adopting the technique detailed in Ref. 7, with two vane pumps, each controlled by an inverter and with flow rate measured by a turbine meter (see Figure 3). The first vane pump transferred the fluid from the saline storage tank into a mixing tank, initially filled with fresh water. Efficient mixing was obtained with a submerged pump located in the mixing tank. The second vane pump transferred the fluid from the mixing tank to the experimental channel. According to Hill,[7] the target flow rates Q_1 and Q_2 in the two circuits are a function of the channel shape and desired density profile, generally vary over time, and are obtained upon solving an inverse problem involving the mass conservation equations for water and salt in the storage and mixing tanks; our formulation of the model includes the dependence of salt water density on salt concentration and temperature. These target flow rates were reached controlling the pumps with a Proportional Integral Derivative (PID) closed loop feedback system acting on the inverters: the turbine meter signal is acquired with a Data Acquisition (DAQ) board and the instantaneous influx rate is compared to the target influx rate. The difference between the measured and the target influx rate is minimized by generating a correction signal to the vane pump rotation rate. The fluid from the mixing tank was injected at the bottom of the channel, employing three pipes of 8 mm internal diameter located in different sections and with a low flow rate (less than 30 $\text{cm}^3\,\text{s}^{-1}$); this setup ensures a limited velocity at the exit section, avoiding excessive mixing, and requires a reasonable time to fill the channel (usually less than 2 h). The density stratification in the channel was measured by extracting samples of $\approx$50 cm^3 volume at 7 different depths using a syringe attached to a needle, whose tip was positioned with a vernier. The density of the samples was measured with a hydrometer with an uncertainty of 10^{-3} g cm^{-3}. The ability of the system to reproduce the requested linear density profile was checked for all the experiments; the agreement between the requested and measured density profiles was very good. Figure 4 shows the experimental density profiles for tanks with (a) semicircular and (b) rectangular cross section. For the constant inflow and for the linearly increasing inflow experiments, it was also necessary to drain the ambient fluid at the end section of the channel (all the experiments are in the configuration of no return flow, with $\gamma = 0$). While in similar experiments with a homogeneous ambient fluid a weir could be efficiently used (see Longo *et al.*[13]), a stratified fluid required an active aspiration system with several small diameter pipes (12 in the present experiments) draining from the whole vertical

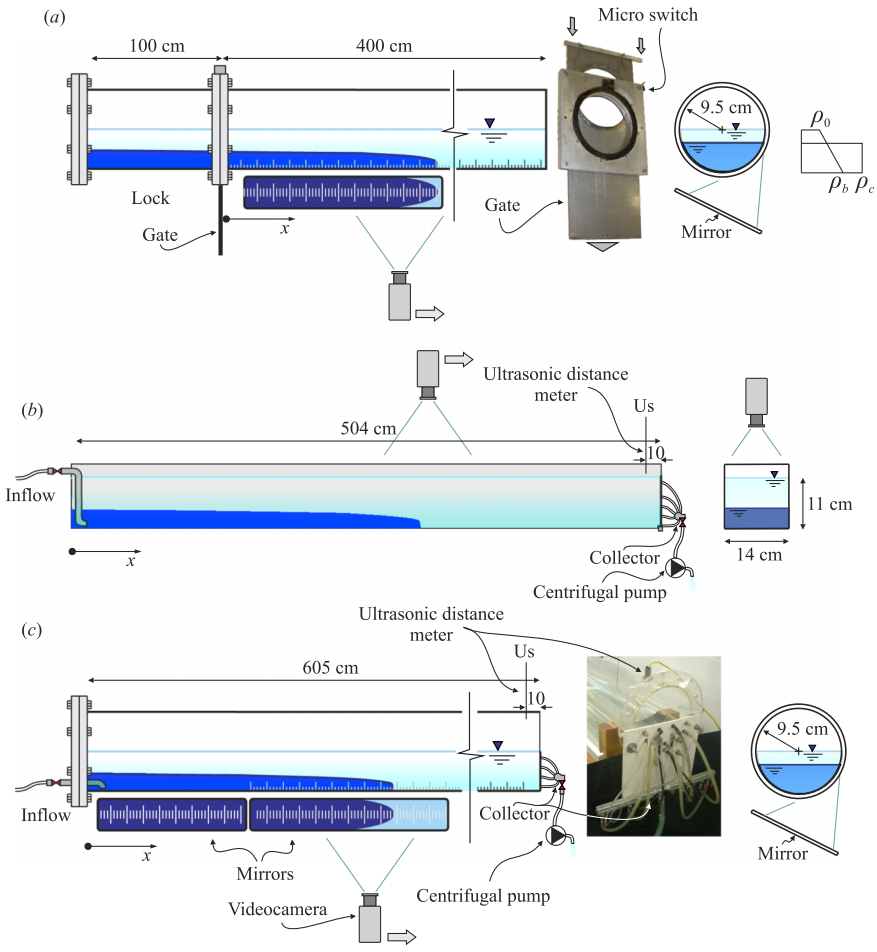

FIG. 2. Schematic of the experimental equipment. (a) Circular channel for lock-release experiments; (b) rectangular and (c) circular channel for constant inflow experiments.

section, in order to avoid the "selective withdrawal" (Koh,[11] Turner[23]). The 12 pipes were connected to a centrifugal pump controlled by an inverter, with a PID feedback chain with the sensor represented by the fluid level recorded by an Ultrasonic distance meter (Turck Banner Q45UR) with an accuracy of 0.03 cm and a time response of 10 ms (see, e.g., Ref. 12 for details). The parameters of

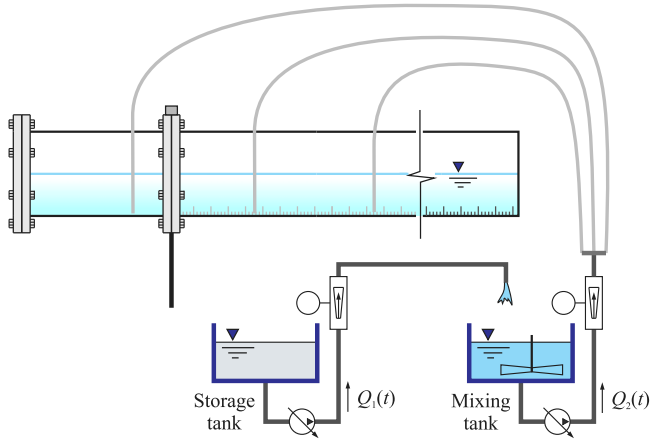

FIG. 3. Schematic of the filling system for generating a stratification in the experimental tank.

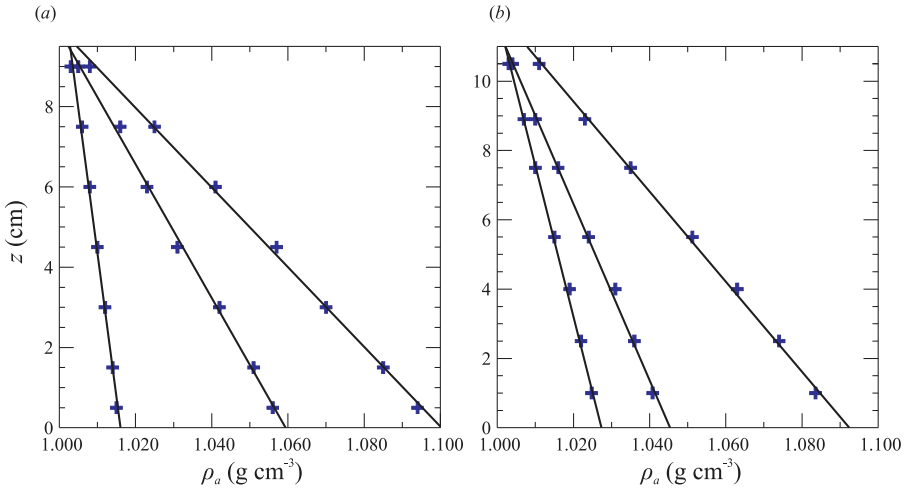

FIG. 4. Typical mass density profiles produced in the experimental tank: (a) semicircular and (b) rectangular cross section.

TABLE I. Parameter values for lock-release experiments in a circular channel. h_0 is the dense current initial depth in the lock, the internal radius is $r = 9.5$ cm, and the ambient fluid depth is $H = r$. $R-1 = (\rho_c - \rho_0)/\rho_0$, $g' = (R-1)g$ is the reduced gravity, $S = (\rho_b - \rho_0)/(\rho_c - \rho_0)$ is the stratification parameter, N is the buoyancy frequency, $Re_0 = U h_0/\nu_c$ is the Reynolds number with ν_c the kinematic viscosity of the denser fluid, and $U = \sqrt{g' h_0}$ and $T = x_0/U$ are the velocity and the time scale, respectively. $x_0 = 100$ cm is the length of the lock. The uncertainty of the measurements and of the parameters is discussed in Sec. III B.

Expt.	h_0 (cm)	$R-1$ (%)	g' (cm s^{-2})	S	N (s^{-1})	Re_0 ($\times 10^3$)	U (cm s^{-1})	T (s)
61	3.2	10.0	98.1	0	0	4.9	17.7	5.645
64	3.2	9.77	95.8	0.287	1.70	4.8	17.5	5.712
57	3.2	9.69	95.0	0.499	2.24	4.8	17.4	5.735
73	3.2	9.33	91.5	0.701	2.60	4.7	17.1	5.845
59	3.2	9.03	88.6	0.873	2.85	4.6	16.8	5.940
70	3.2	9.33	91.5	0.951	3.03	4.7	17.1	5.844
69	3.2	9.48	92.9	0.985	3.10	4.8	17.2	5.799
66	3.2	9.48	93.0	1.000	3.13	4.8	17.3	5.797
54	4	10.0	98.1	0	0	6.8	19.8	5.049
55	4	9.79	96.0	0.274	1.67	6.8	19.6	5.102
49	4	9.77	95.8	0.502	2.25	6.8	19.6	5.108
53	4	9.68	94.9	0.605	2.46	6.7	19.5	5.133
50	4	9.54	93.6	0.706	2.64	6.7	19.3	5.169
51	4	9.28	91.0	0.808	2.78	6.6	19.1	5.241
52	4	9.60	94.2	0.902	2.99	6.7	19.4	5.152
56	4	9.85	96.6	1.000	3.19	6.8	19.7	5.087
63	5	10.0	98.1	0	0	9.5	22.1	4.516
62	5	9.70	95.2	0.290	1.70	9.4	21.8	4.585
58	5	9.78	95.9	0.467	2.17	9.4	21.9	4.566
74	5	9.39	92.1	0.566	2.34	9.3	21.5	4.659
76	5	9.59	94.0	0.583	2.40	9.3	21.7	4.613
60	5	9.68	94.9	0.770	2.77	9.4	21.8	4.590
67	5	9.54	93.6	0.842	2.88	9.3	21.6	4.623
71	5	9.53	93.4	0.912	2.99	9.3	21.6	4.626
65	5	9.60	94.2	0.942	3.06	9.4	21.7	4.609
75	5	9.55	93.7	0.937	3.04	9.3	21.6	4.621
72	5	9.49	93.1	0.958	3.06	9.3	21.6	4.635
68	5	9.39	92.1	1.000	3.12	9.3	21.5	4.659

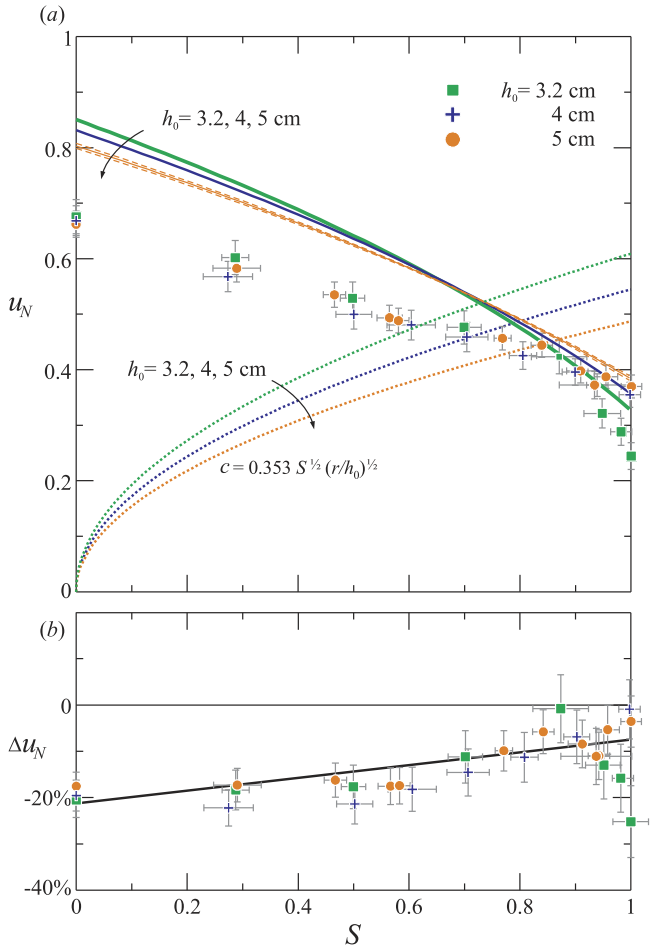

FIG. 5. Circular channel, lock-release experiments. (a) The experimental speed of the GC front during the slumping phase (symbols), compared with the theoretical predictions (curves). The dashed curves delimit the confidence band of the model. The theoretical celerity of internal waves $c = 0.353 S^{1/2}(r/h_0)^{1/2}$ is also shown (dotted curves) for the three different values of h_0. (b) The relative error of the experimental speed $u_{N-\mathrm{exp}}$ with respect to the theoretical prediction $u_{N-theory}$, $\Delta u_N = (u_{N-\mathrm{exp}} - u_{N-theory})/u_{N-theory}$. The line is an interpolation of the relative errors for the three series of experiments. The error bars indicate one standard deviation.

the PID were adjusted in order to guarantee a limited variation of the free surface level near the end section of the channel.

The current fluid was salt water added with aniline dye and had a mass density equal to 1.100 g cm^{-3} in all the experiments except in the 6 experiments with linearly increasing inflow ($\alpha = 2$), where the mass density was 1.060–1.080 g cm^{-3}.

The position of the current front was measured with a full HD video camera (Canon Legria HF 20, 1920 × 1080 pixels) with a data rate of 25 fps. The video camera was moved parallel to the pipe or from the top of the rectangular channel in order to get the nose of the current in the Field of View (FOV). A grid stuck to the bottom allowed the referencing of the front position, with an overall uncertainty of 0.2 cm.

For the lock-release experiments conducted in the circular channel, a gate was opened fast after filling the lock and the downstream pipe. A micro-switch closed by the gate gave the trigger signal to an LED visible in the Field of View (FOV) of the video camera in order to get the time reference. For the constant inflow experiments and for the linearly increasing inflow experiments, a pipe with its axis parallel to the channel was inserted into the channel and connected to a centrifugal pump controlled by an inverter. The flow rate was thus measured through a turbine meter with an overall accuracy equal to 1% of the instantaneous value.

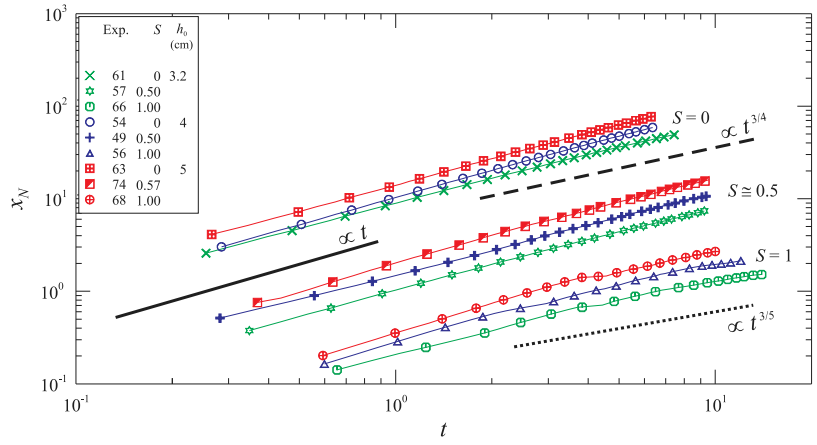

FIG. 6. The distance of propagation of the currents measured from the gate lock section for lock-release in the circular channel for some experiments. The solid line represents the similarity solution with $x_N \propto t$, the dashed line represents the self-similar solution in inertial-buoyancy regime for $S = 0$ with $x_N \propto t^{3/4}$, and the dotted line represents the self-similar solution in inertial-buoyancy regime for $S = 1$ with $x_N \propto t^{3/5}$. The data of different experiments have been decimated and translated in the vertical for a better visualization.

A series of special experiments was devoted to the measurements of the internal waves in the circular channel. The synthetic schlieren method described in Ref. 5 was used, with a mask of randomized array of dots mimicking the tracers in Particle Image Velocimetry (PIV) technique and positioned between the light source and the channel. The video camera was in a fixed position on the opposite side of the channel, recording frame by frame the apparent displacement of the fixed dots due to the variation of the refraction index of the fluid. A PIV software was adopted to measure the apparent displacement of the dots, which is proportional to the square of the buoyancy frequency (see, e.g., Ref. 1) and hence is representative of the perturbation of the density field. The spatial resolution achieved with the adopted setup was of less than 0.2 cm. Some tests were performed with a Canon EOS full frame 5616×3744 pixels, for a better spatial resolution. The photo-camera was controlled by a PC through a DAQ, taking two pictures per second. The experimental arrangement and the details are given in Appendix C.

TABLE II. Parameter values for constant inflow experiments in a rectangular channel. The width of the channel is $b = 14$ cm and the ambient fluid depth is $H = 11$ cm. $Re_0 = UH/\nu_c$ is the Reynolds number with ν_c the kinematic viscosity of the denser fluid, $U = \sqrt{g'H}$ and $T = H/U$ are the velocity and the time scale, respectively, and Q is the influx rate made dimensionless with respect to H^2U. All the experiments are in no return flow condition, with $\gamma = 0$. For other symbols, see caption of Table I.

Expt.	Q	$R-1$ (%)	g' (cm s^{-2})	S	N (s^{-1})	Re_0 ($\times 10^3$)	U (cm s^{-1})	T (s)
38	0.036	10.0	98.1	0	0	31.1	32.8	0.335
36	0.037	9.46	92.8	0.165	1.18	30.3	31.9	0.344
35	0.037	9.55	93.6	0.291	1.57	30.4	32.1	0.343
34	0.038	9.18	90.0	0.439	1.90	29.8	31.5	0.350
32	0.038	9.25	90.7	0.636	2.29	30.0	31.6	0.348
33	0.038	9.11	89.3	0.782	2.52	29.7	31.3	0.351
37	0.038	9.13	89.6	0.916	2.73	29.8	31.4	0.350
45	0.020	10.0	98.1	0	0	31.1	32.8	0.335
43	0.020	9.76	95.7	0.257	1.49	30.8	32.4	0.339
44	0.021	9.62	94.4	0.317	1.65	30.6	32.2	0.341
41	0.021	9.64	94.5	0.491	2.05	30.6	32.2	0.341
39	0.021	9.37	91.9	0.689	2.40	30.2	31.8	0.346
42	0.021	9.41	92.3	0.691	2.41	30.2	31.9	0.345
46	0.020	9.71	95.3	0.888	2.77	30.7	32.4	0.340

B. Uncertainty in measurements and parameters

The mass density of the fluid was measured by a hydrometer with an uncertainty of 10^{-3} g cm^{-3}. The correspondent uncertainty for the stratification parameter $S = (\rho_b - \rho_0)/(\rho_c - \rho_0)$ is $\Delta S/S$ = 1.6%–8.5%. The level of the ambient fluid was detected with an accuracy of 0.1 cm inducing a relative uncertainty $\Delta H/H \leq 1.1\%$ and $\Delta\beta/\beta \leq 2.2\%$ by assuming that the radius of the channel had an absolute uncertainty of 0.1 cm. The velocity scale had an uncertainty $\Delta U/U \leq 2.4\%$ and the time scale had an uncertainty equal to $\Delta T/T = 3.4\%$. The influx rate was measured with uncertainty equal to 1% of the instantaneous value and the dimensionless influx rate had an uncertainty equal to $\Delta Q/Q \leq 5.5\%$. By assuming an uncertainty of 1% in the value of the kinematic viscosity of the dense fluid, the Reynolds number had an uncertainty equal to $\Delta Re/Re \leq 5.2\%$.

The uncertainty in the front speed measurements has been assumed equal to the uncertainty of the angular coefficient of the line interpolating the front position at different time. Most measurements are affected by an uncertainty ≤6.0%, a few have an uncertainty ≤10.0%.

The uncertainty analysis has also been extended to the theoretical model, by assuming that the model parameters are affected by a known uncertainty. A Monte Carlo simulation has been performed by describing the parameters as random variables with Gaussian distribution, with

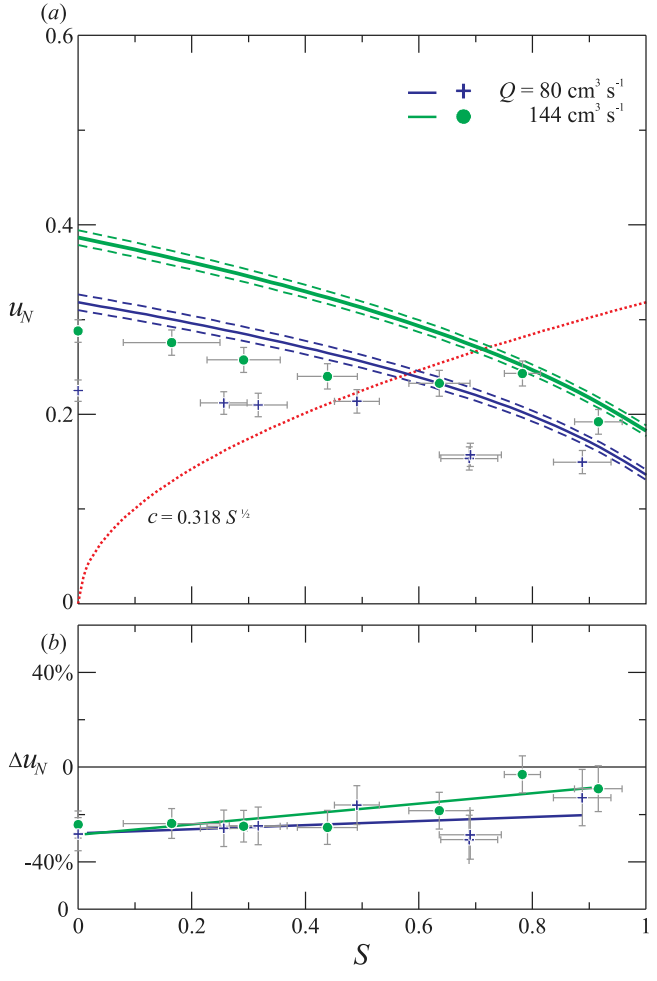

FIG. 7. Rectangular channel, constant inflow experiments. (a) The experimental speed of the GC front during the slumping phase (symbols), compared with the theoretical predictions (curves). The dashed curves delimit the confidence band of the model. The dotted curve of equation $c = 0.318S^{1/2}$ is the theoretical celerity of internal waves (Baines[2]). (b) The relative error of the experimental speed $u_{N-\exp}$ with respect to the theoretical prediction $u_{N-theory}$, $\Delta u_N = (u_{N-\exp} - u_{N-theory})/u_{N-theory}$. The two lines are an interpolation of the relative errors for the two series of experiments. The error bars indicate one standard deviation.

samples of 1000 elements. The variability of the theoretical model predictions is represented by bands corresponding to one standard deviation of the population of output data.

C. Results and discussion

Table I lists the parameters for the lock-release experiments in a circular channel, with three different values of h_0 and several different values of the stratification parameter S. Figure 5(a) shows the theoretical and the experimental front speed against S. The initial Reynolds number was larger than ≈4600 ensuring an inviscid regime for most of the space travelled by the current. The front speed decreases for increasing S and follows the theoretical parabolic reduction. The relative error shown in Figure 5(b) is always less than 30% and is generally negative (i.e., the experimental front speed is smaller than the theoretical one) except for $S > 0.8$. For experiments with the minimum initial depth in the lock ($h_0 = 3.2$ cm), also corresponding to the minimum Reynolds number, for $S > 0.9$ the error increases again, presumably due to the viscosity effects. In order to evaluate the effects of internal waves, their theoretical celerity is also drawn. The theoretical celerity of internal waves is computed according to the model detailed in Appendix C, and is equal to $c = Nr/(2\sqrt{2})$ (dimensional values). The dimensionless counterpart is $c = S^{1/2}/(2\sqrt{2})(r/h_0)^{1/2}$, where $(r/h_0)^{1/2}$ derives from the adopted velocity scale.

The GCs of the present experiments are generally in supercritical regime (the front speed is greater than the wave celerity), except for $S \to 1$, where the front speed and the internal waves celerity become comparable. Figure 6 shows the distance of propagation for some selected

TABLE III. Parameter values for constant inflow experiments in a circular channel. The internal radius is $r = 9.5$ cm, the channel length is $l = 605$ cm, and the ambient fluid depth is $H = r$. $Re_0 = UH/\nu_c$ is the Reynolds number with ν_c the kinematic viscosity of the denser fluid, $U = \sqrt{g'H}$ and $T = H/U$ are the velocity and the time scale, respectively, and Q is the influx rate made dimensionless with respect to H^2U. All the experiments are in no return flow condition, with $\gamma = 0$. For other symbols, see caption of Table I.

Expt.	Q	$R-1$ (%)	g' (cm s^{-2})	S	N (s^{-1})	Re_0 ($\times 10^3$)	U (cm s^{-1})	T (s)
11	0.052	10.0	98.1	0	0	25.0	30.5	0.311
8	0.053	9.68	95.0	0.136	1.16	24.6	30.0	0.316
9	0.053	9.75	95.6	0.268	1.64	24.7	30.1	0.315
10	0.053	9.75	95.6	0.278	1.67	24.7	30.1	0.315
7	0.053	9.80	96.1	0.287	1.70	24.7	30.2	0.314
14	0.054	9.36	91.7	0.444	2.07	24.2	29.5	0.322
15	0.053	9.59	94.0	0.534	2.30	24.5	29.9	0.318
12	0.053	9.72	95.3	0.583	2.42	24.6	30.1	0.316
6	0.053	9.77	95.8	0.591	2.44	24.7	30.2	0.315
17	0.054	9.38	91.9	0.619	2.45	24.2	29.6	0.321
13	0.054	9.46	92.7	0.624	2.47	24.3	29.7	0.320
16	0.053	9.69	95.0	0.632	2.51	24.6	30.0	0.316
24	0.055	9.10	89.3	0.691	2.55	23.8	29.1	0.326
48	0.053	9.79	96.0	0.791	2.83	24.7	30.2	0.315
47	0.054	9.37	91.9	0.820	2.82	24.2	29.5	0.322
28	0.054	9.34	91.5	0.852	2.86	24.2	29.5	0.322
30	0.055	9.18	90.1	0.871	2.87	24.0	29.3	0.325
25	0.024	10.0	98.1	0	0	25.0	30.5	0.311
26	0.024	9.45	92.7	0.276	1.64	24.3	29.7	0.320
19	0.024	9.89	97.0	0.462	2.17	24.9	30.4	0.313
20	0.025	9.19	90.1	0.565	2.32	24.0	29.3	0.325
18	0.024	9.41	92.3	0.574	2.36	24.2	29.6	0.321
21	0.025	9.22	90.5	0.695	2.57	24.0	29.3	0.324
22	0.024	9.60	94.1	0.781	2.78	24.5	29.9	0.318
27	0.025	8.88	87.1	0.899	2.87	23.6	28.8	0.330
31	0.024	9.65	94.6	0.926	3.04	24.6	30.0	0.317

experiments in a log-log plot with decimated experimental points and with a vertical translation of the three groups (corresponding to the three different values of h_0) for a better visualization. The solid line indicates the constant speed in the slumping phase, whereas the other two lines refer to the self-similar solutions for the $S = 0$ case with $x_N \propto t^{3/4}$ (see Ref. 14 for more experiments with $S = 0$), and the $S = 1$ case with $x_N \propto t^{3/5}$. The behaviour is regular, with reduced front speed for increasing S. In particular, the three experiments with $S = 1$ show an evident change of front speed at $t \approx 4$, with a progressive adaptation to the dotted curve. The overall agreement between theory and experiments is very good.

The parameters for the experiments with constant inflow ($\alpha = 1$) in a rectangular channel are reported in Table II. The experimental (symbols) and the theoretical (lines) front speed for two different influx rates and for different values of the stratification parameter S are shown in Figure 7(a). The theoretical curve correctly interprets the experiments, with larger speed for larger influx rate and smaller S. The theoretical celerity of the internal waves is also represented in the same plot. It is computed according to the theoretical value for the first mode, $c = NH/\pi$ (dimensional value, see Ref. 2); the latter is made non-dimensional with respect to U and expressed as a function of the stratification parameter as $c = S^{1/2}/\pi \equiv 0.318S^{1/2}$. For $S < 0.6$–0.7 the current is supercritical, while it becomes subcritical for $S \to 1$. However, there is no evidence of a significant effect of the

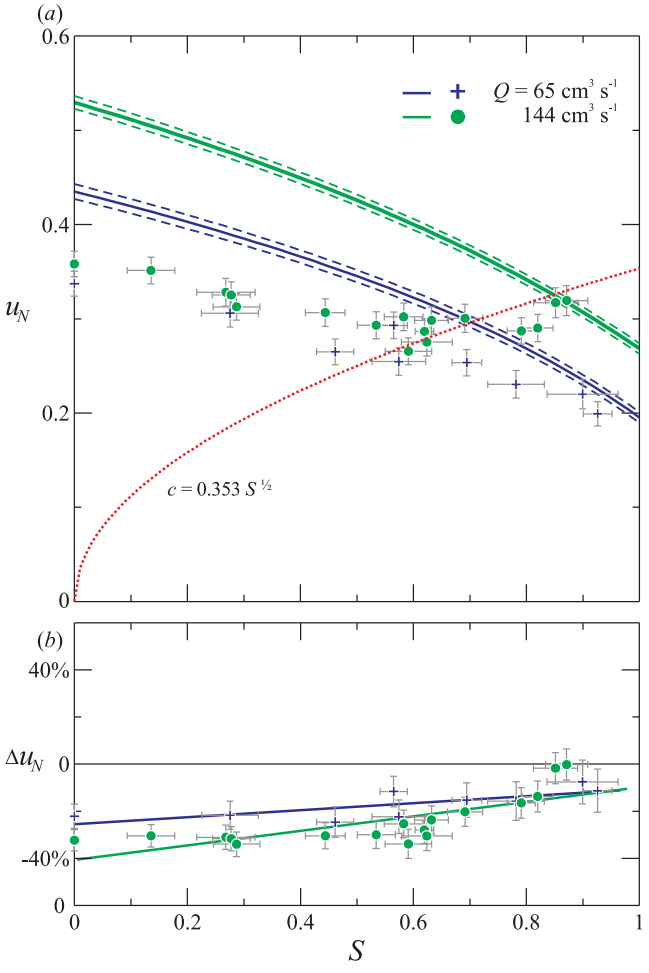

FIG. 8. Circular channel, constant inflow experiments. (a) The experimental speed of the GC front during the slumping phase (symbols), compared with the theoretical predictions (curves). The dashed curves delimit the confidence band of the model. The dotted curve of equation $c = 0.353S^{1/2}$ is the theoretical celerity of internal waves. (b) The relative error of the experimental speed $u_{N-\mathrm{exp}}$ with respect to the theoretical prediction $u_{N-theory}$, $\Delta u_N = (u_{N-\mathrm{exp}} - u_{N-theory})/u_{N-theory}$. The two lines are an interpolation of the relative errors for the two series of experiments. The error bars indicate one standard deviation.

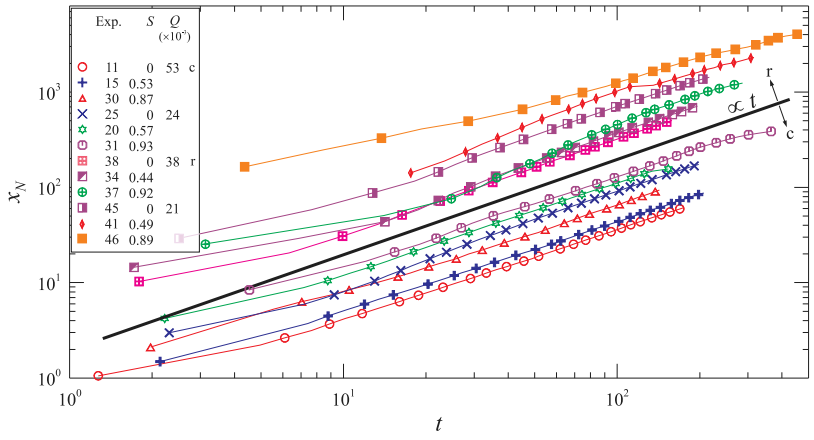

FIG. 9. The distance of propagation of the currents measured from the inlet for circular and rectangular cross section channel for some experiments. Different data symbols correspond to different experiments with a constant Q at the source. The solid line represents the slumping phase with $x_N \propto t$. The data of different experiments have been decimated and translated in the vertical for a better visualization.

internal waves on the front speed. The relative error, shown in Figure 7(b), is generally less than 30% and reduces for $S \to 1$.

The parameters for the third set of experiments (constant inflow in a circular cross section) are listed in Table III. Some experiments are characterized by identical values in order to check the repeatability. The comparison between theory and experiments is shown in Figure 8(a). The trend (a decreasing front speed for increasing S) is correctly captured for the two series with different influx rates. A comparison with the theoretical celerity of internal waves shows a different behaviour for the two series: the experiments with lower influx rate (Q = 65 cm^3 s^{-1}) are apparently unaffected by the internal waves, whereas the experiments with larger influx rate (Q = 144 cm^3 s^{-1}) show a remarkable influence of the internal waves. The front speed increases in subcritical regime and almost equals the celerity of the internal waves. Figure 8(b) reports the relative error in the front speed, which reduces for increasing values of the stratification parameter S and is generally less than ≈30% and less than ≈40% for the lower and the higher influx rate experiments. The correct interpretation of the different behaviour of the two series of experiments requires a coupling analysis between the front of the current and the internal waves, and is beyond the capability of the simplified theoretical model used here.

Figure 9 shows the distance of propagation of some selected experiments with constant inflow for rectangular and circular cross section, respectively. The solid line indicates the theoretical solution with $x_N \propto t$; it is seen that after an initial adjustment the experiments show a remarkable agreement with the theory.

TABLE IV. Parameter values for linearly increasing inflow experiments ($\alpha = 2$) in a circular channel, for $S = 0$ and $S = 1$. The theoretical self-similar solution predicts $x_N \propto t^{5/4}$ and $x_N \propto t^{7/5}$, respectively. For symbols, see caption of Table III. Q is made dimensionless with respect to HU^2.

Expt.	Q (×10^{-5})	$R-1$ (%)	g' (cm s^{-2})	S	N (s^{-1})	Re_0 (×10^3)	U (cm s^{-1})	T (s)
87	2.8	6.00	58.8	0	0	19.4	23.6	0.402
88	4.7	6.00	58.8	0	0	19.4	23.6	0.402
89	6.6	6.00	58.8	0	0	19.4	23.6	0.402
86	2.1	8.13	79.7	1	2.89	22.5	27.5	0.345
84	3.5	8.16	80.0	1	2.90	22.6	27.6	0.345
85	4.7	8.38	82.2	1	2.94	22.9	27.9	0.340

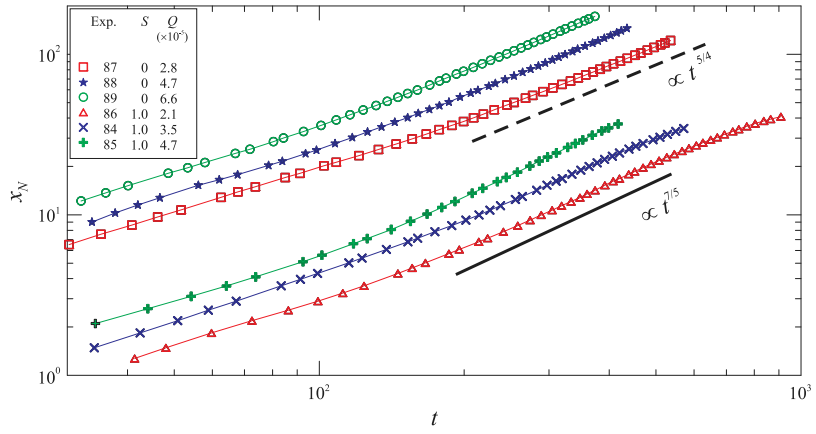

FIG. 10. The distance of propagation of the currents for the circular channel for three experiments with $S = 0, 1$ and a linearly increasing influx ($\alpha = 2$). The dashed and solid lines represent the theoretical self-similar behaviour with $x_N \propto t^{5/4}$ ($S = 0$) and $x_N \propto t^{7/5}$ ($S = 1$).

Table IV lists the parameter for two special series of experiments in a circular cross section channel, with $S = 0$ and $S = 1$, respectively. The inflow rate is linearly increasing in time ($\alpha = 2$), a condition which allows self-similar propagation. The comparison with the theoretical front speed is shown in Figure 10, where the experimental asymptotic front position (symbols) follows the theoretical front position (bold and dashed lines) with a satisfactory agreement.

IV. CONCLUSIONS

We investigated the behaviour of high-Reynolds-number gravity currents that propagate into a linearly stratified ambient. Several configurations were analyzed, considering the following currents: (i) released from a lock or sustained by a constant or variable source; (ii) flowing in channels of different shapes (rectangular or circular); and (iii) intruding into ambients with a different stratification parameter S. The study is focused on laboratory experiments, whose results were compared with predictions of shallow-water models; for some of these, a novel formulation was obtained as an extension of earlier models. The main novelty of our work is the non-rectangular shape of the cross section, and the enhanced experimental equipment. We used a 605 cm long tank, with a special arrangement of pumps that ensured a smooth withdrawal of the stratified fluid at the outflux boundary. Special attention was given to the internal-stratification waves. This enhances the confidence in the accuracy of our observations. To provide additional support to the theory, experiments were performed also in a tank with standard rectangular cross section. To the best of our knowledge, experiments with constant inflow in a stratified ambient fluid in a rectangular cross section channel are also a novelty. A last set of experiments was devoted to self-similar currents in circular cross section. Self-similarity is confirmed, within the uncertainty of the experiments, for $S = 0$ and $S = 1$ and time varying influx ($\alpha = 2$).

In general, the propagation of the current is in fair agreement with the theoretical predictions. The significant influence of the stratification parameter S and cross-section shape was confirmed by the experiments. In accord with theory, a lock-released current displays a "slumping" stage of propagation with constant u_N, whose value decreases as the stratification S increases. The theory overestimates u_N typically by 20%–30%, which is consistent with previously published counterpart results for non-stratified and rectangular-container systems. The speed of propagation of the influxed current displays the same behavior. However, for large-influx cases, an unexpected deviation was noticed: at some larger values of S, the speed slightly increases with S. This discrepancy is attributed to the influence of the internal waves; the available theoretical models assume an unperturbed ambient, and do not account for this influence. This interaction between the waves and the gravity current supported by influx is an interesting and complicated topic whose investigation must be left for future studies. Some disturbances are also attributed to the free surface perturbations

(see Ref. 13) which affect the ambient fluid dynamics and induce further discrepancies between the theoretical model (a fixed lid is assumed in the model) and the experiments. A further refinement of the model shall be based on corrections for the shape of the velocity profiles, for mixing and entrainment effects, for energy dissipation. In particular, mixing effects are expected to be particularly relevant for a truly 3-D flow of a GC in a circular cross section. In view of all these disturbing effects, the experimental relative differences with the theory are very limited and give confidence of the correctness of the simplifying assumptions and of the strength of the model. We highlight that the circular shape of the cross section does not merely imply a slight modification of the equations in the models, and it is not clear *a priori* if the new geometry can be treated in the same way of the classical flat-bottom current. Also, the internal waves propagate with a close feedback from the geometry of the channel, due to the wall reflections: in all situations where the interaction between gravity currents and internal waves is relevant, the results are expected to be strongly dependent on the shape of the cross section.

APPENDIX A: GEOMETRICAL EXPRESSIONS FOR A CIRCULAR CROSS SECTION

The Froude number can be expressed as

$$Fr^2 = \frac{2(1-\varphi)}{1+\varphi}\left[1-\varphi+\frac{J(h)}{hA(1)}\right], \tag{A1}$$

$$\varphi = A(h)/A(1), \tag{A2}$$

where h is the depth of the current, $A(h)$ the area occupied by the current, $A(1)$ the area occupied by the ambient fluid, and $J(h)$ a function of h, all in dimensionless form. For a circular cross section with a fixed given radius, represented by $y = f(z) = (2rz - z^2)^{1/2}$ (r is the dimensionless radius), $A(h)$ and $J(h)$ are

$$A(h) = \int_0^h 2(2rz-z^2)^{1/2}dz = \left[(h-r)(2rh-h^2)^{1/2} - r^2\arcsin(1-h/r) + \frac{\pi}{2}r^2\right], \tag{A3}$$

$$J(h) = 2\int_0^h (2rz-z^2)^{1/2}z\,dz = -\frac{2}{3}(2rh-h^2)^{3/2} + rA(h). \tag{A4}$$

APPENDIX B: ANALYTICAL MODEL FOR INTERNAL WAVES

Internal waves in finite-depth channels were examined by Yih[34] (circular and elliptic cross section) and Baines[2] (rectangular cross section). However, the analysis by Yih does not recover the dispersion equation of the waves. Here we recall the scheme and then evaluate the celerity of the long waves.

We consider a circular cross section channel fully filled with a continuously stratified fluid. Let u, v, and w be the velocity components along x, y and z, respectively, with x denoting the pipe axis (assumed horizontal), z along the vertical and y perpendicular to both x and z. The centre of the circle is at $z = 0$. The pressure is p and the density is ρ. The variables are decomposed into a (time) average and a fluctuating component, indicated by a bar and a prime, respectively,

$$u = \bar{u} + u', \tag{B1a}$$

$$v = \bar{v} + u', \tag{B1b}$$

$$w = \bar{w} + u', \tag{B1c}$$

$$\rho = \bar{\rho} + \rho', \tag{B1d}$$

$$p = \bar{p} + p', \tag{B1e}$$

where $d\bar{p}/dz = -g\,\bar{\rho}$, and g is the acceleration of gravity. In the following we limit our analysis to a fluid at rest, with zero average velocities.

By neglecting terms at lower orders, the linear momentum equations for inviscid fluids read

$$\bar{\rho}u'_{,t} = -p'_{,x}, \tag{B2a}$$

$$\bar{\rho} v'_{,t} = -p'_{,y}, \tag{B2b}$$

$$\bar{\rho} w'_{,t} = -p'_{,z} - g\rho', \tag{B2c}$$

where the subscript indicates the partial derivative. The continuity equation is represented by

$$\rho'_{,t} + \rho\,(u'_{,x} + v'_{,y} + w'_{,z}) + w'\bar{\rho}_{,z} = 0, \tag{B3}$$

with the incompressibility equation (see Ref. 34),

$$\rho'_{,t} + w'\bar{\rho}_{,z} = 0. \tag{B4}$$

Hence the continuity equation (B3) reads

$$u'_{,x} + v'_{,y} + w'_{,z} = 0. \tag{B5}$$

By assuming that the fluctuating terms are proportional to $e^{-i\omega t}$, where ω is the circular frequency, (B2) and (B4) become

$$u' = \frac{p'_{,x}}{i\omega\bar{\rho}}, \tag{B6a}$$

$$v' = \frac{p'_{,y}}{i\omega\bar{\rho}}, \tag{B6b}$$

$$w' = \frac{p'_{,z} + g\rho'}{i\omega\bar{\rho}}, \tag{B6c}$$

$$w' = \frac{i\omega\rho'}{\bar{\rho}_{,z}}, \tag{B6d}$$

where (B6c) and (B6d) yield

$$w' = -i\omega\frac{p'_{,z}}{\bar{\rho}\omega^2 + g\bar{\rho}_{,z}}. \tag{B7}$$

Combining (B6) with (B5) yields

$$p'_{,xx} + p'_{,yy} + \omega^2\bar{\rho}\left(\frac{p'_{,z}}{\omega^2\bar{\rho} + g\bar{\rho}_{,z}}\right)_{,z} = 0. \tag{B8}$$

If we consider a linear density stratification of the form $\bar{\rho}(z) = \rho_0(1 - \beta z)$ with a weak dependence on z, within the Boussinesq approximation (i.e. $\rho_0/\bar{\rho} \approx 1$), Eq. (B8) reads

$$p'_{,xx} + p'_{,yy} + \frac{\omega^2}{g\beta - \omega^2}p'_{,zz} = 0. \tag{B9}$$

By assuming the pressure fluctuation as a disturbance propagating along x,

$$p'(x, y, z) = f(y, z)e^{ikx}, \tag{B10}$$

where k stands for the wavenumber and f has the dimension of a pressure, Eq. (B9) reads

$$f_{,yy} - \lambda^2 f_{,zz} - k^2 f = 0, \tag{B11}$$

where

$$\lambda^2 = \frac{\omega^2}{g\beta - \omega^2}. \tag{B12}$$

If $\mathsf{F}(x, y, z) = 0$ is the generic function describing the boundary, the kinematic condition at the boundary reads

$$\mathsf{F}_{,x}p_{,x} + \mathsf{F}_{,y}p_{,y} - \lambda^2\mathsf{F}_{,z}p_{,z} = 0 \quad \text{on } \mathsf{F} = 0, \tag{B13}$$

which for a circular cross section channel $\mathsf{F} \equiv y^2 + z^2 - r^2 = 0$ yields

$$y f_{,y} - \lambda^2 z f_{,z} = 0 \quad \text{on } \mathsf{F} = 0. \tag{B14}$$

In order to solve the partial differential equation (B11) with the boundary condition (B14), it is convenient to introduce the new coordinates (μ, ν),

$$y = r\frac{\sin\mu\sin\nu}{\sin\alpha}, \quad z = r\frac{\cos\mu\cos\nu}{\cos\alpha}, \tag{B15}$$

where $\omega/\sqrt{g\beta} = \cos\alpha$ and α is in the range $[0, \pi/2]$. In the new coordinates μ-ν, the internal part of the circle $y^2 + z^2 - r^2 < 0$ becomes the rectangle $-\alpha \le \mu \le \alpha$, $\alpha \le \nu \le \pi - \alpha$, and the four segments,

$$\begin{cases} \mu = -\alpha, & \alpha \le \nu \le \pi - \alpha, \\ \mu = \alpha, & \alpha \le \nu \le \pi - \alpha, \\ \nu = \alpha, & -\alpha \le \mu \le \alpha, \\ \nu = \pi - \alpha, & -\alpha \le \mu \le \alpha, \end{cases}$$

map the circle. The governing Equation (B11) becomes

$$f_{\mu\mu} - f_{\nu\nu} - \frac{k^2r^2}{2\cos\alpha}\left(\cos 2\nu - \cos 2\mu\right) f = 0. \tag{B16}$$

The boundary condition (B14) reads

$$\frac{\partial f}{\partial \mu} = 0, \quad \text{at } \mu = -\alpha, \alpha, \tag{B17a}$$

$$\frac{\partial f}{\partial \nu} = 0, \quad \text{at } \nu = \alpha, \pi - \alpha. \tag{B17b}$$

A possible solution can be expressed as $f(\mu, \nu) = F(\mu)G(\nu)$ and Eq. (B16) is split into the system

$$F'' - (a - q\cos 2\mu)F = 0, \tag{B18a}$$

$$G'' - (a - q\cos 2\nu)G = 0, \tag{B18b}$$

in which $q = -k^2r^2/2\cos^2\alpha$ and a is a constant arising from the separation of variables.

The equations (B18) are the canonical form of the Mathieu equations. The solution is reported in Yih,[34] with α obtained by the boundary conditions in Eq. (B17), but the dispersion relation is not computed.

In order to find the dispersion relation, we recall the solution obtained for the cosine-type functions by considering $m = 0$ (see Ref. 15, Sec. 2.150]),

$$F = 1 - \frac{1}{2}q\cos 2\mu + \frac{1}{32}q^2\cos 4\mu + O(q^3), \tag{B19a}$$

$$G = 1 - \frac{1}{2}q\cos 2\nu + \frac{1}{32}q^2\cos 4\nu + O(q^3). \tag{B19b}$$

Imposing the boundary conditions neglecting the terms $O(q^3)$ results in

$$\left.\frac{dF}{d\mu}\right|_{\mu=\pm\alpha} \equiv \pm\left(q\sin 2\alpha - \frac{1}{8}q^2\sin 4\alpha\right) = 0, \tag{B20a}$$

$$\left.\frac{dG}{d\nu}\right|_{\nu=\alpha,\pi-\alpha} \equiv \pm\left(q\sin 2\alpha - \frac{1}{8}q^2\sin 4\alpha\right) = 0, \tag{B20b}$$

with the solution,

$$q = \frac{4}{2\cos^2\alpha - 1}. \tag{B21}$$

Substituting $q = -\frac{k^2r^2}{2\cos^2\alpha}$ with $\cos\alpha = \omega/\sqrt{g\beta}$ in Eq. (B21) yields

$$c = \frac{r\sqrt{g\beta}}{\sqrt{8 + 2r^2k^2}}. \tag{B22}$$

The buoyancy frequency $N^2 = -(g/\rho)\partial\rho/\partial z$ for a linearly stratified fluid becomes $N^2 \approx g\beta$ by means of the Boussinesq approximation, and Eq. (B22) gives

$$c = \frac{Nr}{\sqrt{8 + 2r^2k^2}} \tag{B23}$$

equal to

$$c = \frac{Nr}{2\sqrt{2}} \text{ for } k \to 0 \tag{B24}$$

in the long wave approximation. For comparison, we recall that the first mode of long hydrostatic internal waves in a fluid at rest into a rectangular channel of height H has a celerity (Baines[2]),

$$c_{rect} = \frac{NH}{\pi}, \tag{B25}$$

and propagates faster than in the circular cross section of radius $r = H/2$.

If we consider a semi-circle with a lid at the top, we can still use the transformation (B15) with the rectangle in the $\mu - \nu$ plane $-\alpha < \mu < \alpha$, $\pi/2 < \nu < \pi - \alpha$. The semicircle is represented by the function $\mathsf{F}(y,z) \equiv z - \sqrt{r^2 - y^2} = 0$ with $-r < y < r$ and the lid by the function $\mathsf{F}_l(y,z) \equiv z = 0$ with $-r < y < r$.

The boundary condition (B13) then becomes

$$y f_{,y} - \lambda^2 z f_{,z} = 0 \quad \text{on } \mathsf{F} = 0, \quad z < 0, \tag{B26}$$

$$f_{,z} = 0 \quad \text{on } \mathsf{F}_l = 0 \quad -r < y < r. \tag{B27}$$

It can be demonstrated that adopting the same approach already used for the full circle, the celerity has still the expression given by Eq. (B23).

Let us continue the analysis about internal waves in circular channels. We deal with the following solutions of F and G:

$$F = 1 - \frac{1}{2} q \cos 2\mu + \frac{1}{32} q^2 \cos 4\mu + O(q^3), \tag{B28a}$$

$$G = 1 - \frac{1}{2} q \cos 2\nu + \frac{1}{32} q^2 \cos 4\nu + O(q^3), \tag{B28b}$$

which combined yield

$$f = F\,G = (1 - \frac{1}{2} q \cos 2\mu)(1 - \frac{1}{2} q \cos 2\nu) + \frac{1}{32} q^2 \cos 4\mu + \frac{1}{32} q^2 \cos 4\nu + O(q^3). \tag{B29}$$

After some algebra we obtain

$$f = 1 + O(k^2) \tag{B30}$$

or

$$p' = p_0 e^{ikx}, \tag{B31}$$

where p_0 is a constant. From the system (B6), we can compute the fluctuating velocity components u',v', and w',

$$u' = \frac{p'_{,x}}{\bar{\rho} i \omega} = \frac{p_0}{\bar{\rho} c} e^{ikx}, \tag{B32a}$$

$$v' = 0, \tag{B32b}$$

$$w' = 0. \tag{B32c}$$

The results of the system (B32) show that, at the leading order, only the component u' is different from zero and uniform in the cross section.

APPENDIX C: INTERNAL WAVES MEASUREMENTS

In order to check the theoretical model for internal waves celerity in a circular cross section channel, a small set of experiments was performed by generating the internal waves with a small vertical paddle. The experimental arrangement is shown in Figure 11. The images have been processed with a PIV software in order to detect the apparent displacement induced by the fluid density perturbation, proportional to ΔN^2. At a given section, the time series of the apparent displacement

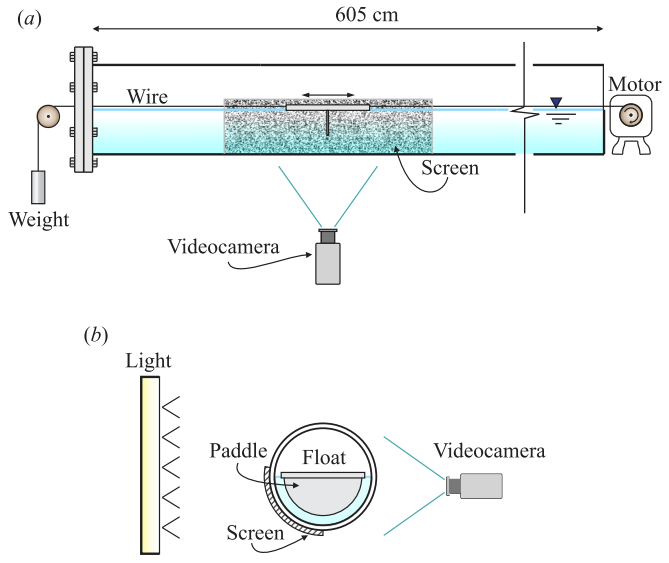

FIG. 11. (a) Front view of the towing apparatus. The motor is at one end of the tank and drives an iron cable balanced by a weight, moving the float with the lid. The imposed motion is periodic; (b) side view of the configuration adopted for applying the synthetic schlieren technique.

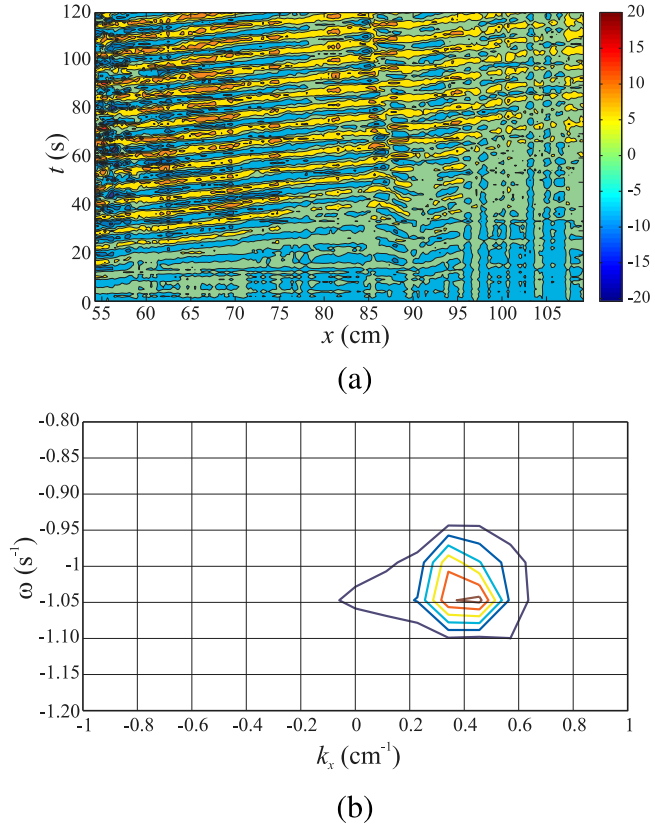

FIG. 12. (a) Sample horizontal time series of the horizontal displacement proportional to ΔN^2. The time series is taken at the vertical location $z = r/2$ in the mid-section of the channel. The bands are the wave crests and troughs which move to the right as time evolves. The imposed period of oscillation is $T = 6$ s. The values in the colorbar are in arbitrary scale; (b) the power spectrum of the signal. The peak of the spectrum has coordinates $\omega_p = 2\pi/6 = 1.05$ s^{-1}, $k_p = 0.45$ cm^{-1}. The ambient fluid has a linear density stratification with $\rho_0 = 1.002$ g cm^{-3} and $\rho_b = 1.022$ g cm^{-3}, with $H = r = 9.5$ cm.

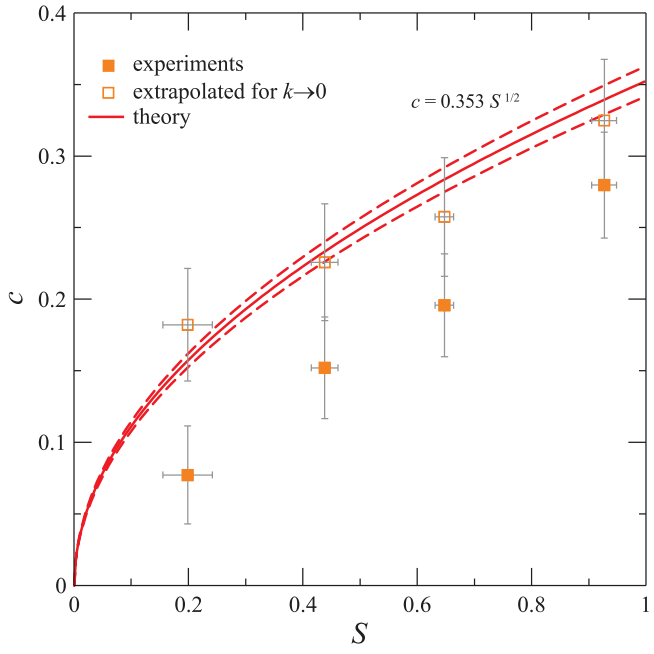

FIG. 13. Internal waves celerity in a circular cross section channel half-filled with a linearly stratified fluid. The experimental data (filled symbols) have been extrapolated to $k \to 0$ (empty symbols). The bold line is the theoretical internal waves celerity in the long wave approximation, and the dashed lines are the 95% confidence limits. The celerity is non-dimensional with respect to $\sqrt{g'H}$, with $H = r = 9.5$ cm, and S is computed with reference to $\rho_c = 1.100$ g cm^{-3}.

is processed with a standard 2-D fast Fourier transform in the domain $\omega - k$ in order to extract the coordinate of the peak (ω_p, k_p), where $\omega = 2\pi/T$ is the imposed pulsation and $k = 2\pi/L$ is the wave number. The imposed pulsation ω_p is computed with reference to the period of oscillation of the paddle; the peak wave number allows the computation of the internal wave celerity, $c(k) = \omega_p/k_p$.

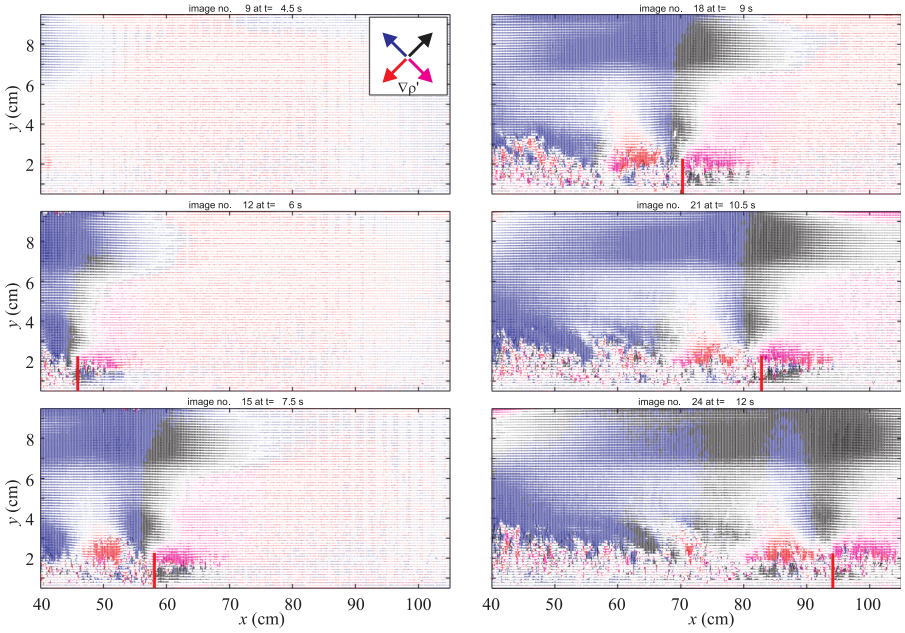

FIG. 14. The visualization of the perturbation of density $\nabla\rho'$ for Experiment 75, a lock-released GC in a circular cross section channel, $S = 0.94$, $N = 3.04$ s^{-1}. The current is subcritical, with $u_{N-\exp} = 0.372 < c = 0.47$. The images are 1.5 s apart, and the vertical red thick line near the bottom indicates the front position.

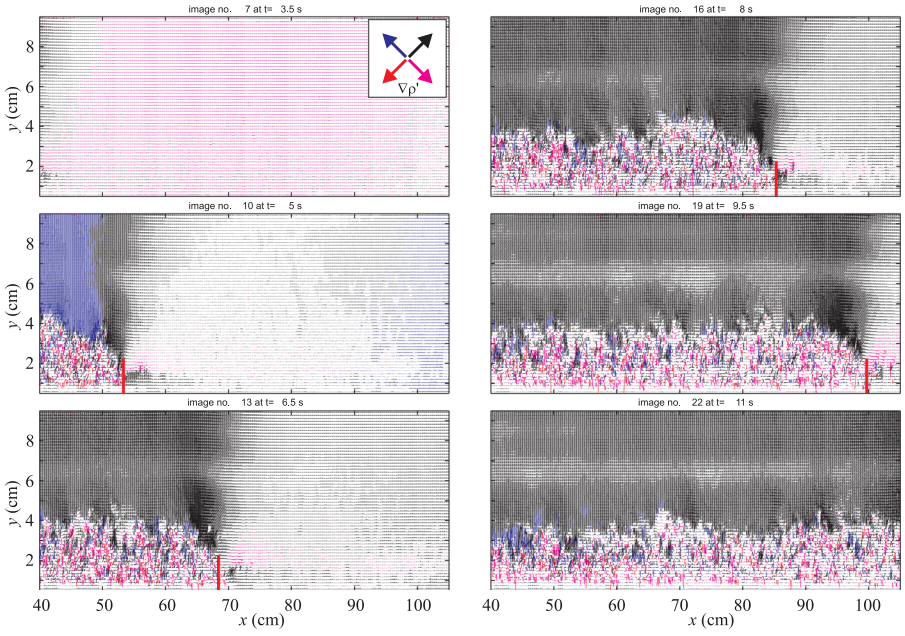

FIG. 15. The visualization of the perturbation of density $\nabla\rho'$ for Experiment 76, a lock-released GC in a circular cross section channel, $S = 0.58$, $N = 2.40\,\mathrm{s}^{-1}$. The current is supercritical, with $u_{N-\mathrm{exp}} = 0.489 > c = 0.37$. The images are 1.5 s apart, and the vertical red thick line near the bottom indicates the front position.

Figure 12 shows the horizontal displacement time series at a given vertical location (ambient fluid mid-depth, $z = r/2$) and the power spectrum. Figure 13 shows the experimental data (filled symbols), corrected to account for $k \neq 0$ in order to estimate the long waves celerity, according to the non-dimensional expression,

$$c_{k\to 0} = c(k)\sqrt{1 + \frac{1}{4}k^2} \tag{C1}$$

where k is made dimensionless with respect to $H = r = 9.5$ cm. The curve is the theoretical internal wave celerity computed in Appendix B. Figs. 14 and 15 show the perturbation of density for Experiment 75 and Experiment 76, respectively, the former with a subcritical current and the latter with a supercritical current. The differences between the two regimes are evident.

[1] D. A. Aguilar, B. R. Sutherland, and D. J. Muraki, "Laboratory generation of internal waves from sinusoidal topography," Deep Sea Res., Part II **53**(1–2), 96–115 (2006).
[2] P. G. Baines, *Topographic Effects in Stratified Flows* (Cambridge University Press, 1997).
[3] T. B. Benjamin, "Gravity currents and related phenomena," J. Fluid Mech. **31**, 209–248 (1968).
[4] J. A. Covault, A. Fildani, B. W. Romans, and T. McHargue, "The natural range of submarine canyon-and-channel longitudinal profiles," Geosphere **7**(2), 313–332 (2011).
[5] B. S. Dalziel, O. G. Hughes, and R. B. Sutherland, "Whole-field density measurements by 'synthetic schlieren,"' Exp. Fluids **28**(4), 322–335 (2000).
[6] M. R. Flynn, M. Ungarish, and A. W. Tan, "Gravity currents in a two-layer stratified ambient: The theory for the steady-state (front condition) and lock-released flows, and experimental confirmation," Phys. Fluids **24**, 026601-1–026601-24 (2012).
[7] F. D. Hill, "General density gradients in general domains: The two-tank method revisited," Exp. Fluids **32**(4), 434–440 (2002).
[8] J. C. R. Hunt, J. R. Pacheco, A. Mahalov, and H. J. S. Fernando, "Effects of rotation and sloping terrain on the fronts of density currents," J. Fluid Mech. **537**, 285–315 (2005).
[9] H. E. Huppert and J. E. Simpson, "The slumping of gravity currents," J. Fluid Mech. **99**, 785–799 (1980).
[10] D. L. Inman, C. E. Nordstrom, and R. E. Flick, "Currents in submarine canyons: An air-sea-land interaction," Annu. Rev. Fluid Mech. **8**(1), 275–310 (1976).
[11] R. C. Y. Koh, "Viscous stratified flow towards a sink," J. Fluid Mech. **24**, 555–575 (1966).
[12] S. Longo, "Experiments on turbulence beneath a free surface in a stationary field generated by a crump weir: Free-surface characteristics and the relevant scales," Exp. Fluids **49**(6), 1325–1338 (2010).
[13] S. Longo, M. Ungarish, V. Di Federico, L. Chiapponi, and F. Addona, "Gravity currents produced by constant and time varying inflow in a circular cross-section channel: Experiments and theory," Adv. Water Resour. **90**, 10–23 (2016).

[14] S. Longo, M. Ungarish, V. Di Federico, L. Chiapponi, and A. Maranzoni, "The propagation of gravity currents in a circular cross-section channel: Experiments and theory," J. Fluid Mech. **764**, 513–537 (2015).
[15] N. W. MacLachlan, *Theory and Application of Mathieu Functions* (Clarendon Press, 1947).
[16] A. Mahalov, J. R. Pacheco, S. I. Voropayev, H. J. S. Fernando, and J. C. R. Hunt, "Effects of rotation on fronts of density currents," Phys. Lett. A **270**(34), 149–156 (2000).
[17] B. M. Marino and L. P. Thomas, "Front condition for gravity currents in channels of nonrectangular symmetric cross-section shapes," J. Fluids Eng. **131**(5), 051201 (2009).
[18] T. Maxworthy, J. Leilich, J. E. Simpson, and E. H. Meiburg, "The propagation of a gravity current into a linearly stratified fluid," J. Fluid Mech. **453**, 371–394 (2002).
[19] J. Monaghan, C. Mériaux, H. Huppert, and J. Monaghan, "High Reynolds number gravity currents along v-shaped valleys," Eur. J. Mech. - B/Fluids **28**(5), 651–659 (2009).
[20] J. W. Rottman and J. E. Simpson, "Gravity currents produced by instantaneous releases of a heavy fluid in a rectangular channel," J. Fluid Mech. **135**, 95–110 (1983).
[21] M. Shringarpure, H. Lee, M. Ungarish, and S. Balachandar, "Front conditions of high-Re gravity currents produced by constant and time-dependent influx: An analytical and numerical study," Eur. J. Mech. - B/Fluids **41**(0), 109–122 (2013).
[22] J. E. Simpson, "Gravity currents in the laboratory, atmosphere, and ocean," Annu. Rev. Fluid Mech. **14**, 213–234 (1982).
[23] J. S. Turner, *Buoyancy Effects in Fluids* (Cambridge University Press, 1973).
[24] M. Ungarish, "On gravity currents in a linearly stratified ambient: A generalization of Benjamin's steady-state propagation results," J. Fluid Mech. **548**, 49–68 (2006).
[25] M. Ungarish, *An Introduction to Gravity Currents and Intrusions* (CRC Press, 2009).
[26] M. Ungarish, "Gravity currents and intrusion of stratified fluids into a stratified ambient," Environ. Fluid Mech. **12**(3), 115–132 (2011).
[27] M. Ungarish, "A general solution of Benjamin-type gravity current in a channel of non-rectangular cross- section," Environ. Fluid Mech. **12**(3), 251–263 (2012).
[28] M. Ungarish, "Two-layer shallow-water dam-break solutions for gravity currents in non-rectangular cross-area channels," J. Fluid Mech. **732**, 537–570 (2013).
[29] M. Ungarish, "Shallow-water solutions for gravity currents in non-rectangular cross-area channels with stratified ambient," Environ. Fluid Mech. **15**(4), 793–820 (2015).
[30] M. Ungarish, "On the front conditions for gravity currents in channels of general cross-section," Environ. Fluid Mech. **16**(4), 747–775 (2016).
[31] M. Ungarish and H. E. Huppert, "On gravity currents propagating at the base of a stratified ambient," J. Fluid Mech. **458**, 283–301 (2002).
[32] M. Ungarish, C. A. Mériaux, and C. B. Kurz-Besson, "The propagation of gravity currents in a V-shaped triangular cross-section channel: Experiments and theory," J. Fluid Mech. **754**, 232–249 (2014).
[33] B. L. White and K. R. Helfrich, "Gravity currents and internal waves in a stratified fluid," J. Fluid Mech. **616**, 327–356 (2008).
[34] C.-S. Yih, *Stratified Flows* (Academic Press, 1980).
[35] T. Zemach and M. Ungarish, "Gravity currents in non-rectangular cross-section channels: Analytical and numerical solutions of the one-layer shallow-water model for high-Reynolds-number propagation," Phys. Fluids **25**, 026601-1–026601-24 (2013).